Cyclic vs Linear Bottlebrush Polymers in Solution: Side Chain Length Effect

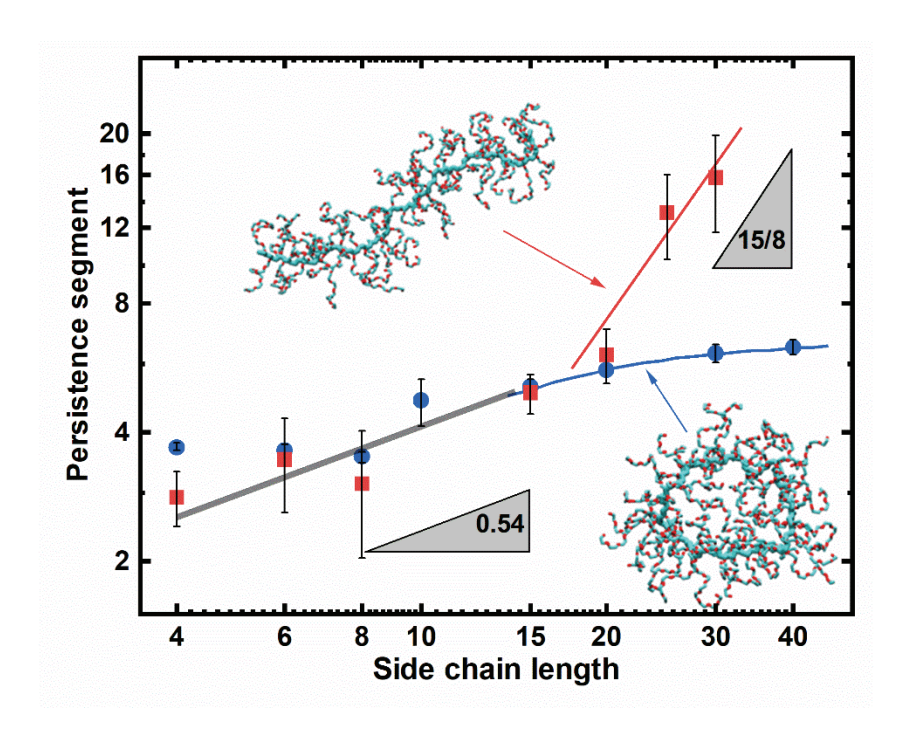
Guang Chen† and Elena E. Dormidontova*,†,‡

†Polymer Program, Institute of Materials Science, University of Connecticut, Storrs, US, 06269

‡Department of Physics, University of Connecticut, Storrs, US, 06269

E-mail: elena@uconn.edu

For Table of Contents use only:



Abstract

Bottlebrush polymers (BBPs) of different architecture are of considerable interest for a broad range of applications, including nanomedicine, electronics, and self-healing materials. Using atomistic molecular dynamics simulations, we investigate and compare the structural and hydration properties of cyclic and linear poly(vinyl alcohol)-graft-poly(ethylene oxide) (PVA-g-PEO_{Nsc}) BBPs in aqueous solution as functions of PEO side chain length, N_{sc}. We find that overall cyclic BBPs are smaller than the corresponding linear BBPs and their shape changes from donut-like to disk-like to star-like with increasing side chain length while linear BBPs vary in shape from expanded coil to a rod/cylinder. The radius of gyration of cyclic BBPs increases with an increase of the side chain length at a somewhat slower rate than the linear BBPs but follows the same scaling $R_g{\sim}N_{sc}^{0.58}$ in the limit of long side chains. For short grafts we determine that the persistence length, l_p , for both cyclic and linear BBPs increases in a similar manner following an $l_p \sim N_{\rm sc}^{0.54}$ dependence. In the long side chain limit, the persistence length (l_p) of cyclic BBP saturates, while for linear BBPs l_p strongly increases following the expected scaling relation $l_p \sim N_{\rm sc}^{15/8}$. We propose a scaling model that shows the side-chain fraction located inside the cyclic BBPs depends on the radius of the backbone ring and significantly decreases with an increase of graft length. For both cyclic and linear BBPs the hydrogen bonding between PEO side chains and water is somewhat reduced near the backbone, where local chain stretching is observed, while reaching full hydration on the periphery. Overall, the hydration shell within 1nm of the cyclic BBP backbone is found to be more dynamically stable compared to linear BBPs.

INTRODUCTION

Bottlebrush polymers (BBPs) have attracted considerable interest due to their unique properties originating from chain architecture¹⁻³ and have found a wide range of applications, such as super soft elastomers,4 nanomedicine,5,6 electronics7 and self-healing materials.⁸ Recently, cyclic BBPs have emerged as a very interesting material. Experiments have established that the difference in backbone topology results in different molecular properties, e.g., cyclic BBPs exhibit a more compact shape and less interchain association^{9,10} than their linear analogs. Although experiments^{6,9-13} as well as dissipative particle dynamics simulations¹⁴ have elucidated many macroscopic properties of cyclic BBPs such as viscosity and self-assembled structures, the molecular level details of structure and dynamics are still missing. Obviously, it would be informative to investigate the similarities and differences in the conformational behavior and properties of cyclic and linear BBPs in order to achieve a fundamental understanding of the chain topology effect. Atomistic simulations can provide such details concerning the structural (e.g., size, shape) and hydration properties of cyclic and linear BBPs. In this manuscript using atomistic molecular dynamics simulations we investigate the structural and hydration properties of cyclic poly(vinyl alcohol)-graftpoly(ethylene oxide) (PVA-g-PEO Nsc) BBP as a function of side-chain length in comparison with the linear analog.

Linear BBPs in solution have been extensively studied experimentally,^{11,13,15,16} theoretically,^{17,18} and by Monte Carlo ^{19–21} and molecular dynamics (MD) simulations.^{22–24} The structure of linear BBPs in melts or networks have also been examined.^{4,25} It is established that the steric interaction of the grafted side chains alters the backbone conformation, causing a coil-to-rod transition upon increasing the length of the side chain.²⁶

It has also been determined that side chain flexibility affects the backbone conformation, namely rigid side chains induce more rigidity to the backbones than flexible ones.²⁰ However, there is still an ongoing debate regarding the effect of side chain length on backbone rigidity for flexible backbones and side chains. A scaling analysis by Birshtein et al.²⁷ and Monte Carlo simulations by Saariaho et al. 20,28,29 indicate only moderate stretching with the persistence length l_p of the backbone scaling as N_{sc}^{ν} (with ν typically in 0.6~0.8). On the other hand, strong stretching of the backbone is expected for long grafts with $l_p{\sim}N_{\rm sc}^{15/8}$ according to Fredrickson²⁶ and confirmed by coarse-grained (CG) MD simulations.¹⁷ Similarly, Subbotin $\it et~al.^{30,31}$ and Nakamura and Norisuye 32 obtained $l_p{\sim}{\rm N_{sc}^2}$ for long grafts. It was argued by Borisov et al. that the lack of strong backbone stretching in computer simulations is attributed to the short graft length 18 typically used in simulations. It is obvious that graft length plays an important role in determining the effective rigidity of the backbone of linear BBPs. However, so far no discussion of the persistence length dependence of cyclic BBPs on the side chain length has been reported in the literature. We will test both limits of short and long side-chains in our atomistic molecular dynamics simulations for cyclic BBPs in comparison to the linear analog. Moreover, for biomedical applications of bottlebrush polymers, e.g., drug delivery, it is important for the BBPs to maintain good hydration, i.e., their ability to form stable hydrogen bonds with water. MD simulations with atomistic resolution and explicit solvent consideration, e.g., water, such as presented in this paper, are necessary to address correctly the conformational and hydration properties of BBPs.

Using atomistic MD simulations with explicit water, we investigate the structural and hydration properties of hydrophilic poly(vinyl alcohol)-graft-poly(ethylene oxide) BBPs with cyclic and linear backbones. In the results presented here we consider the high grafting

density limit: one graft per repeat unit of backbone and vary the graft length N_{sc} over the range $4{\sim}40$ to cover the short and long graft range (experimentally²² N_{sc} < 100) with a backbone length N_{bb} =50. We investigate how the backbone topology and graft length affect the chain conformation, rigidity, and overall shape of linear and cyclic BBPs. We also analyze the hydration of the side chains near and away from the backbone and how quickly water exchanges near the backbone for BBPs of different architecture. Understanding these conformational and hydration differences can provide fundamental insights and be useful in guiding experimental design of hydrophilic bottlebrush-based nanomaterials.

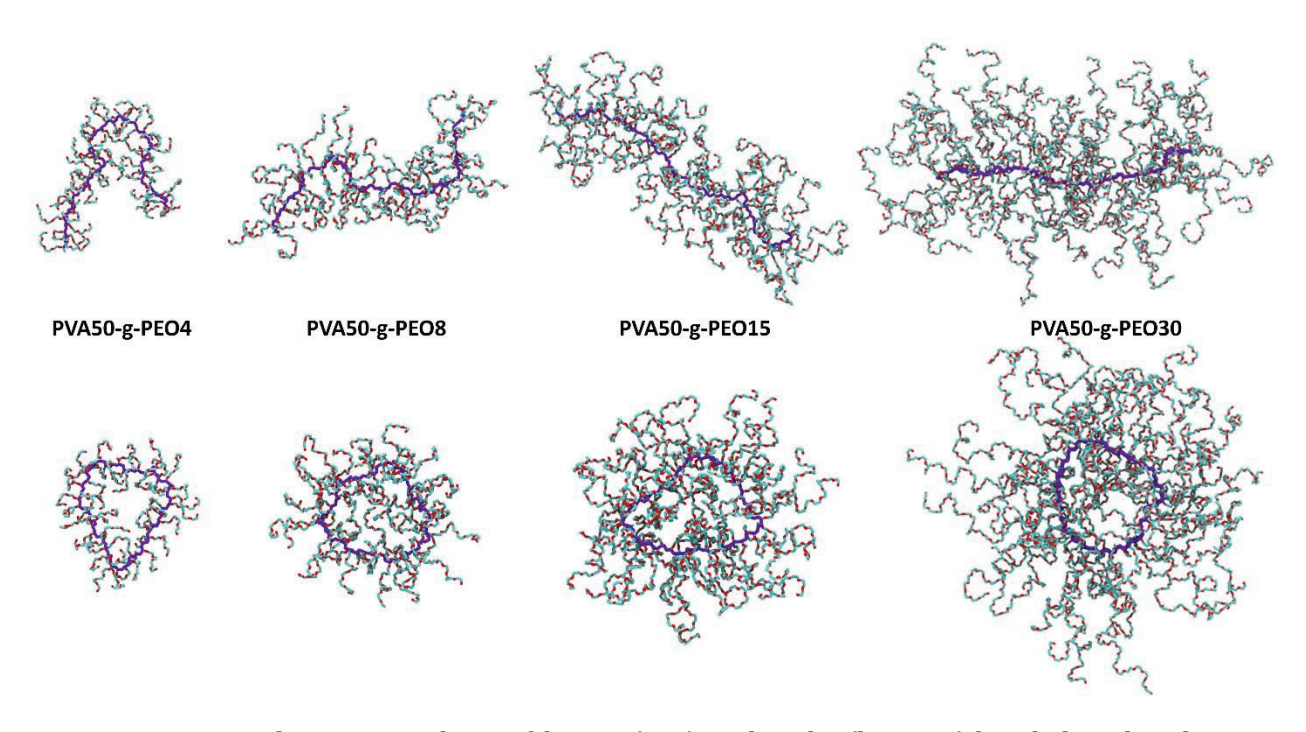


Figure 1: MD simulation snapshots of linear (top) and cyclic (bottom) bottle brush polymers differing in PEO side chain lengths: N_{sc} =4, 8, 15, and 30. The PVA backbone (N_{bb} = 50) is shown in violet, the PEO side chains are in cyan (carbon) and red (oxygen). Water is not shown for clarity. The snapshots were produced using VMD.³³

SIMULATION DETAILS

The atomistic molecular dynamics simulations of dilute aqueous solutions of cyclic and linear PVA-g-PEO bottlebrush polymers were performed using Gromacs 2020.4 with GPU acceleration³⁴ on the Extreme Science and Engineering Discovery Environment (XSEDE)³⁵ and the Advanced Cyberinfrastructure Coordination Ecosystem: Services & Support (ACCESS). Linear and cyclic bottle brushes with PVA backbone of 50 repeat units (terminated by methyl groups for linear BBPs) were studied. Each PVA repeat unit was grafted with a PEO side chain of 4 to 40 repeat units terminated by a hydroxyl group. The OPLS-AA force field³⁶ was used for PVA backbone and modified OPLS-AA force field for PEO to correctly reproduce the conformation and hydration properties.³⁷ Each simulation setup contained a single linear or cyclic BBP solvated in SPC/E water³⁸ corresponding to dilute solutions. The box size (with periodic boundary conditions applied in all directions) varied depending on the system size to ensure at least 3 nm distance between polymers and the boundary. The minimum and maximum box sizes are listed in Table S1 in the Supporting Information. All systems were firstly equilibrated in an NPT ensemble for at least 10 ns using the Berendsen thermostat with a time constant of 0.1 ps at 300K and the Berendsen barostat with a time constant of 5.0 ps at 1 bar pressure. For the production run at least 200 ns for the linear BBPs (300 ns for N_{sc}≥6) and more than 100 ns for the cyclic BBPs were used with the V-rescale thermostat and the Parrinello-Rahman barostat (with the same parameters as that in the initial equilibration stage). A 1.0 nm cutoff was used for short-range pair and electrostatic interactions. The long-range correction for the pair interactions was applied for the pressure and energy calculation, and the long-range electrostatic interactions were

calculated by the PME method with a Fourier spacing of 0.12 nm. A time step of 2 fs was used with the LINCS bond constraint enforced for all chemical bonds with hydrogens.

For data analysis, we used the standard Gromacs modules to characterize the structural and hydration properties such as the radius of gyration, end-to-end distances, persistence length (using *gmx polystat* in Gromacs), and hydrogen bonding (the distance between a donor and the acceptor less than 0.35 nm and the angle between a hydrogen atom of water, the oxygen atom of the same water, and the acceptor of PEO oxygen atoms less than 30°). For side chain stretching, the hydration number and water residence correlation function calculation we employed VMD tcl/tk scripting.³³

RESULTS AND DISCUSSION

Characteristic sizes of the bottlebrush polymers. Typical equilibrated structures of linear and cyclic PVA-g-PEO bottle brush polymers with different PEO side chain lengths are shown in Figure 1. One can see that the backbones of the linear BBPs become more rigid upon increasing the PEO side chain length, consistent with many previous studies.^{1,2} For cyclic BBPs the backbone also becomes more elongated, but the overall structure remains more compact compared to the linear counterpart. Previous experiments have shown that cyclic BBPs are more compact and assume a smaller hydrodynamics volume than the corresponding linear ones.⁹ To quantitatively compare the range of conformations that bottle brushes explore, we calculated the frequency distribution of the radius of gyration (Rg) of the cyclic and linear BBPs, shown in Figure 2. For both BBPs, the Rg increases with an increase of the side chain length, while the cyclic BBPs have a narrower distribution than their linear counterparts, as the linear BBPs have a larger range of possible conformations. Furthermore, as the side chain length increases, the width of the Rg distribution increases along with the average Rg value for cyclic BBPs, while for the linear BBP the distribution

becomes narrower as the backbone assume a more rigid-rod shape that is less susceptible to conformational changes until side chain contribution starts to dominate and distribution width starts to increase (for N_{sc} =30) We note that in the limit of very long side-chains (N_{sc} >> N_{bb}) both cyclic and linear BBPs are expected to behave like star polymers (with a more compact core for cyclic BBPs) and the distributions for linear and cyclic PPBs will coincide.

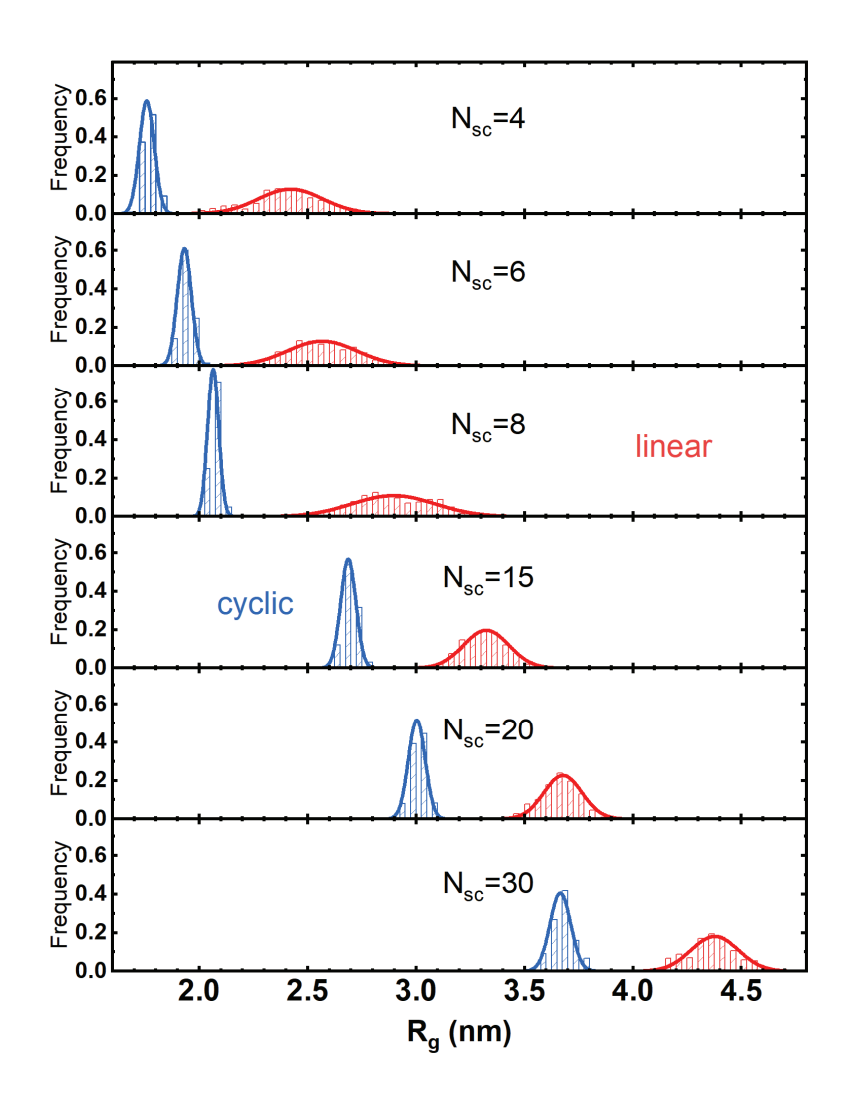


Figure 2: Frequency distribution for the radius of gyration for cyclic (blue) and linear (red) BBPs with different side chain lengths: N_{sc} =4, 6, 8, 15, 20, and 30 from the top to the bottom.

To quantify the dependence of the R_g on the side chain length, we show in Figure 3 the average Rg of the whole BBPs as a function of the side chain length. Overall, it demonstrates that the R_g of both BBPs increase with the side chain length, consistent with the images shown in Figure 1. One can also see that the R_g of cyclic BBPs is smaller than that of its linear analog, consistent with experimental observations ¹³ for linear poly(chloroethyl vinyl ether)graft-polystyrene BBPs with N_{bb} in 500~900 and N_{sc}=100 and 170. Furthermore, cyclic and linear BBPs have a somewhat similar two-regime dependence of R_g on the side chain length. For short grafts the contribution from side chains to $R_{\mbox{\scriptsize g}}$ is weaker than from the backbone, as the backbone-backbone excluded volume interactions dominate.²⁶ In this regime, the R_g of cyclic BBPs scales as $R_g \sim N_{sc}^{0.22}$, while R_g of linear BBPs agrees within error bars with the $N_{sc}^{0.36}$ scaling reported in experiments and predicted by mean-field theory. ^{39,40} For example, Rouault and Borisov 39 obtained a $R_g \sim N_{sc}^{0.36}$ scaling for linear BBPs using a Flory-type mean field approach, and Pan et al.40 found the same scaling experimentally using linear poly(propargyl acrylate)-graft-polystyrene bottlebrush polymers in a good solvent condition for 620<N_{bb}<1780 and 17<N_{sc}<150. The difference in scaling exponents between cyclic and linear BBPs is likely attributed to the stronger conformational limitations for the backbone of cyclic BBP. For long grafts, the side chains contribute more to the Rg of BBPs as discussed in more detail below and the R_g scales as $R_g \sim N_{sc}^{0.58}$ for cyclic BBP and approaches this scaling for linear BBPs in the long graft limit. This scaling is consistent with experimental observations for linear BBPs with long grafts in solution.^{41,42} For example, Zhang et al.⁴¹ obtained a scaling exponent $v = 0.57 \pm 0.05$ for chemically identical backbone and side chain monomers using poly(t-butyl acrylate) and poly(n-butyl acrylate) at a high grafting density in THF (good solvent condition) with N_{sc} in the range 28~157. In addition, Zhang et al.⁴² found ν = 0.56~0.67 using polymethacrylate-graft-polystyrene bottlebrushes (N_{sc} in the range 6~33) in toluene and cyclohexane (good solvent condition).

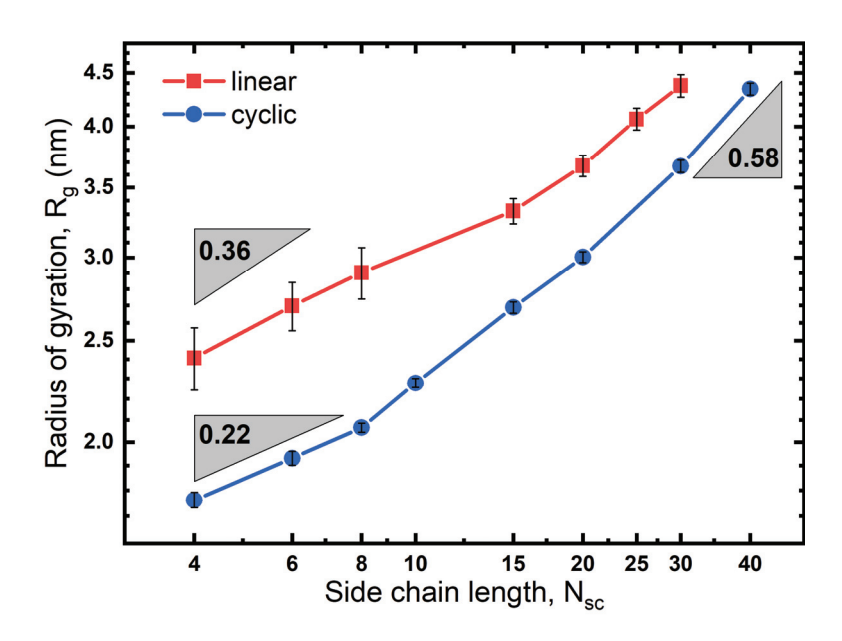


Figure 3: The average radius of gyration of the cyclic (blue) and linear (red) bottlebrush polymers as functions of the side chain length N_{sc} (log-log scale).

For cyclic BBPs, in the limit of long grafts, the snapshots of our MD simulations show that BBPs enters the star polymer regime where $R_g \sim N_{sc}^{\nu}$ is expected with ν being the scaling exponent expected for a linear chain of the same polymer in solution.^{43,44} For PEO in aqueous solutions, ν =0.6 was reported by atomic MD simulations⁴⁵ and ν =0.583 by experiments.⁴⁶ Therefore, our MD simulation results for the radius of gyration for the linear and cyclic BBPs agree well with both experiments and previous MD simulations of linear BBPs, indicating that for a given backbone length with much longer grafts (N_{sc} >> N_{bb}) both cyclic and linear BBPs are expected to behave like star polymers.

To examine the structural change of the backbone upon side chain length increase, we calculated the radius of gyration of the backbone, shown in Figure 4a. One can see that the radius of gyration of the backbone of linear BBPs increases firstly with side chain increase, and then saturates at the long side chain limit, in qualitative agreement with previous CGMD

simulations of a poly(norbornene)-graft-poly(lactide) (PNB-g-PLA) linear bottlebrush. ¹⁵ In contrast, Rg of cyclic BBP backbone firstly remain practically unchanged and then increases exhibiting a less significant change compared to the linear ones, as is seen in Figure 4a, due to the topology constraint of the backbone ring (no free chain ends). To rationalize the difference in the behavior of the backbone R_g's, the principle components of the backbone $R_{g,bb}$ were analyzed $(R_{g1,bb} \ge R_{g2,bb} \ge R_{g3,bb})$ as functions of graft length, as shown in Figure S1 of the Supporting Information. For cyclic BBPs the largest component Rg1 decreases with an increase of side chain length, while the $R_{\rm g2}$ increases compensating each other (with the smallest component R_{g3} remaining constant) that results in the plateau of Rg for the cyclic backbone for N_{sc}≤8 in Figure 4. In other words, the backbone becomes more circular and less anisotropic, as will be discussed below. Upon further increase in N_{sc} the smallest component R_{g3} starts to decrease as well leading to an increase in R_{g,bb}. In contrast, for linear BBPs, the largest component Rg1 increases as the backbone expands from a coil to rod-like and the other two components decrease resulting in an increase of both R_{g,bb} and the aspect ratio for the backbone of linear BBPs (Figure S2) of the Supporting Information. This indicates that the backbone of cyclic BBPs becomes more ring-like and the linear backbone is more rod-like as the graft length increases, as is further analyzed below using a dimensionless scaling comparison.

We evaluated the ratio of the radius of gyration of the linear backbone to that of the cyclic backbone, which provides insights on the effect of grafted chains on the rigidity of the backbone, as shown in Figure 4b. One can see that this ratio at N_{sc} =4 is close to $\sqrt{2}$ (yellow dashed line), which is expected for the ratio of R_g 's of an ideal linear and a cyclic polymer of the same length N without grafts:⁴⁷

$$\frac{R_{g,linear}}{R_{g,cyclic}} = \frac{N^{1/2}b/\sqrt{6}}{N^{1/2}b/\sqrt{12}} = \sqrt{2}$$
 (1)

where b is the Kuhn segment length. This implies a rather weak effect of grafting for BBPs with short grafts, which can also be observed from the equilibrated structures shown in Figure 1. With an increase of the side chain length the backbones of both cyclic and linear BBPs approach their long-graft limit, ring- and rod-like, respectively and thereby the ratio for linear and cyclic bottle brush polymers reaches a plateau of $\pi/\sqrt{3}$ (magenta dashed line in Figure 4b) corresponding to the ratio between R_g 's of a rod and a perfect ring:

$$\frac{R_{g,rod}}{R_{g,ring}} = \frac{Nb/\sqrt{12}}{Nb/2\pi} = \frac{\pi}{\sqrt{3}}$$
 (2)

A rod-like structure for the linear BBP is seen from the snapshot in Figure 1 and follows from the dependence of the end-to-end distance and the aspect ratio for the backbone of the linear BBPs, as shown in Figure S2 in the Supporting information. The end-to-end distance increases and saturates with the side chain length increase, while the aspect ratio increases from about $\sqrt{6}$ (expected for a coil) to $\sqrt{12}$ (expected for a rod).⁴⁷

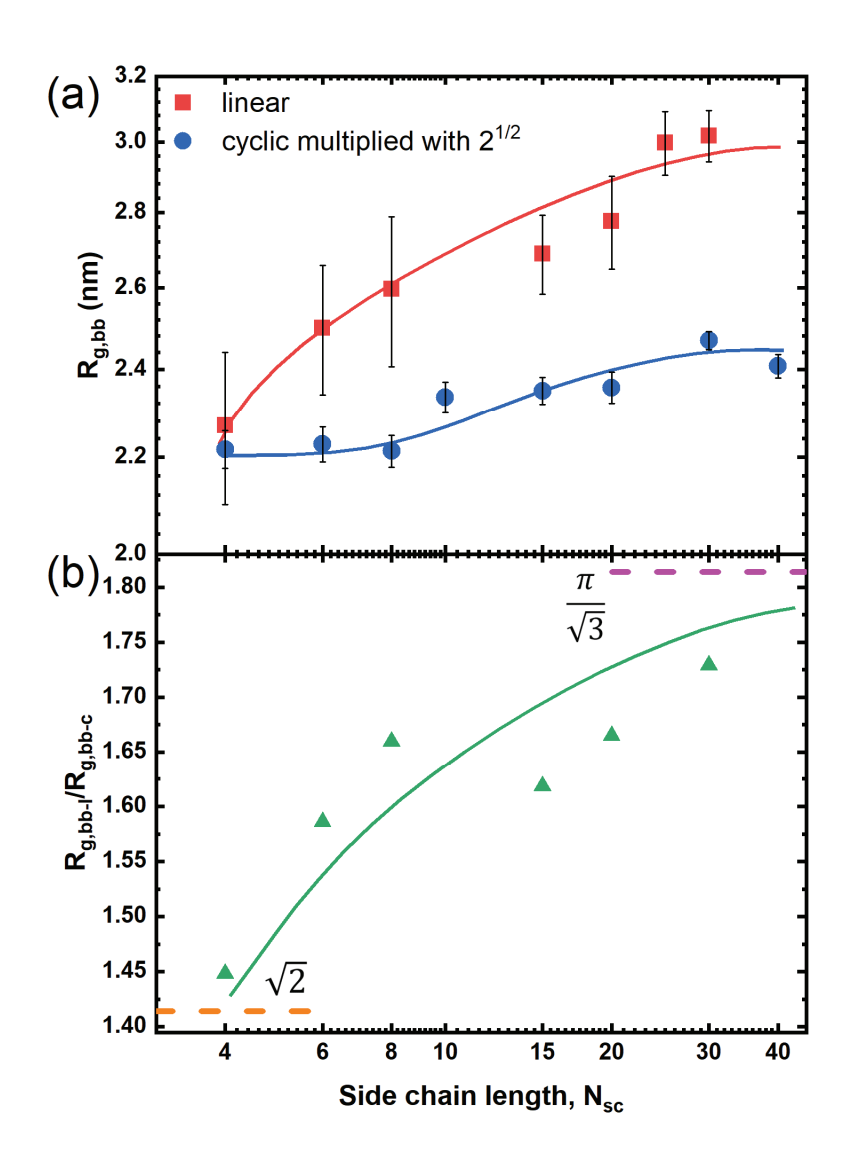


Figure 4: (a) The backbone radius of gyration of the linear and cyclic bottlebrush polymers as a function of the side chain length N_{sc} (log-log scale). R_g for the cyclic BBP is scaled by a factor $\sqrt{2}$. (b) The ratio of the backbone radius of gyration of the linear and cyclic BBPs as a function of the side chain length N_{sc} in a semi-log scale. Yellow dashed line shows $\sqrt{2}$ and magenta dashed line $\pi/\sqrt{3}$ limits according to Eqs. (1) and (2). Lines in both plots are guides for the eye.

It is therefore evident that the backbone for both cyclic and linear BBPs gains rigidity upon side chain length increase. To quantify this change, we calculated the persistence length (in terms of the number of monomers) for the backbones, as shown in Figure 5. For short grafts $(N_{sc} \le 20)$, in the limit of a long backbone, $N_{bb} >> 1$, there should be a negligible difference

between the persistence lengths l_p for cyclic and linear BBPs which follow $l_p{\sim}N_{sc}^{0.54}\,\text{,}$ indicating that for short grafts the backbone gains similar rigidity locally. We note that for a finite backbone length as in this work, the backbone ring topology may induce a higher initial rigidity for cyclic BBPs compared to the linear PPBs that could lead to a somewhat slower rigidity increase for cyclic BBPs with graft length. The shorter the backbone of a cyclic BBP the larger deviation from the linear chain behavior can be expected. For the longer grafts, there are distinctive scaling differences between cyclic and linear BBPs. In the case of cyclic BBPs the persistence length saturates at a long graft limit as the backbone approaches a perfect circle and is constrained by the curvature of the backbone ring $l_{p,long}=N_{bb}\frac{\theta}{2\pi}$ with $cos\theta = e^{-1}$ related to the bond-bond correlation function decay (Equation S3 and Figure S3 of the Supporting Information). On the contrary for the linear BBPs the persistence length drastically increases for side chains lengths exceeding 20 (N_{sc}>20), i.e., when it exceeds about half the backbone length (N_{bb}=50). We note that for the longest side chains the persistence length for a linear BBP is of the same order of magnitude as the contour length of the backbone, for which the calculation is less accurate. 16,42 Nonetheless, in the long side chain limit ($N_{sc}>20$) in Figure 5 we observe the scaling exponent of 15/8 for the persistence length. Similar results have been obtained by Chatterjee and Vilgis¹⁷ using CG simulations for linear BBPs based on the bead spring model: the scaling of the persistence length changes with the graft length including 15/8 exponent in the long side-chain limit. The change of the persistence length of linear BBPs from short to long grafts was predicted by a theoretical model by Fredrickson,²⁶ who reported a 3/5 exponent for short grafts and 15/8 in the long graft limit. Similarly, Subbotin and Semenov³¹ and Nakamura and Norisuye³² predicted a $l_p \sim N_{sc}^2$ scaling for the long grafts based on a free energy analysis.

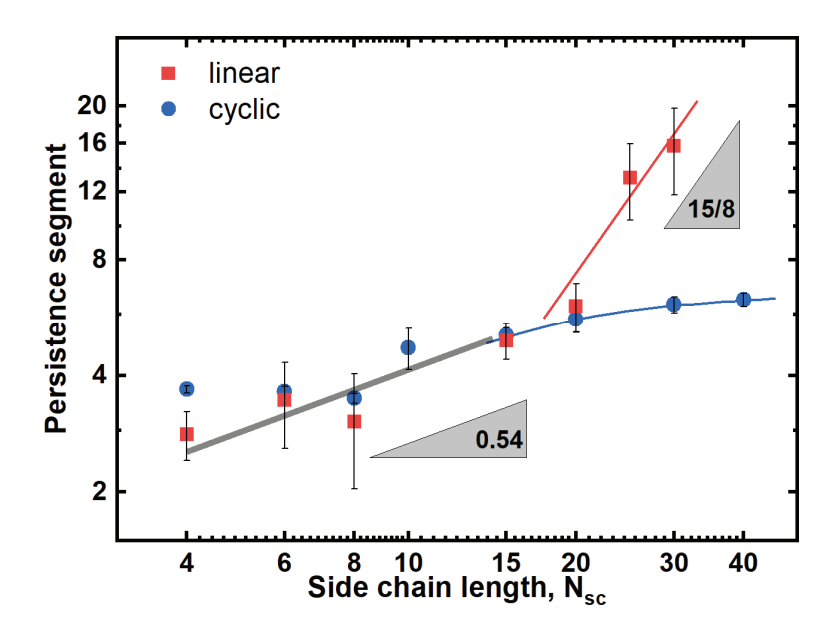


Figure 5: Log-log plot of the persistence length of the backbone of the cyclic (blue circle) and linear (red square) BBPs as a function of the side chain length. Grey line is the fit for short side chains, red line is for the linear BBPs and blue line for cyclic BBPs for long side chains. The blue line is a guide for the eye.

In addition to the structural change of the backbone induced by a side chain length increase, it is also interesting to investigate if the difference in the backbone topology affects the side chain conformation. To that end, we have calculated the mean-square distance between the oxygen closest to backbone to oxygens along the side chain as a function of the oxygen index starting from the backbone, as shown in Figure 6. One can see that the data for side chains grafted on cyclic and linear backbones almost perfectly overlap and correspondingly show comparable scaling characteristics: $R_{end,sc} \sim N_{sc}^{0.8}$, except for the end segments (last two repeat units) which bend back in order to participate in intramolecular hydrogen bonding via the end hydroxyl group. This scaling is similar to $\nu = 3/4$ predicted by a self-consistent field theory (SCFT) for poly(L-lysine)-graft-poly(ethylene glycol), $\nu = 0.64$ obtained in CGMD simulations of PNB-g-PLA system, $\nu = 0.68$ found in a Monte Carlo simulation of CG bottlebrush polymers ($\nu = 0.68$ found in a didition, the radius of gyration of PEO follows a $\nu = 0.68$ scaling, as shown in Figure S4 of the Supporting Information. This indicates a

slightly stretched chain conformation, compared to $R_{g0} \sim N^{0.583}$ of PEO in aqueous solutions found experimentally⁴⁶ and $N^{0.60}$ in previous MD simulations.⁴⁵ This scaling is also consistent with CGMD simulations of PNB-g-PLA linear BBPs in dilute solution that demonstrated a $R_{g,sc} \sim N_{sc}^{0.70}$ scaling²³ and experimental observations⁴¹ reporting a $N_{sc}^{0.67}$ scaling for poly(t-butyl acrylate) BBPs (with chemically identical backbone and side chains and N_{sc} in the range 28~157).

Comparing the radius of gyration of PEO side chain of $N_{sc} = 20$ of linear or cyclic BBPs to that of a single linear PEO chain in an aqueous solution, we found that $R_{g,sc}/R_{g0} = 1.1$ (where $R_{g0}=0.92$ nm for PEO in an aqueous solution⁴⁵), while for the longest chains studied, $N_{sc} = 30$, the aspect ratio $R_{end,sc}/R_{g,sc}$ is about 2.8, only slightly larger than 2.4 expected for a coil-like chain but much smaller than 3.5 expected for a rod-like chain conformation (Figure S5 in the Supporting Information). Our observations are consistent with previous scaling analysis and CGMD simulations of linear BBPs which showed that the side chains are only weakly stretched.⁴⁸ In fact, when plotting the expansion ratio $\alpha^2 = r^2/r_0^2$ of neighboring oxygen-to-oxygen mean-square distance (r^2) along PEO side chains to that for PEO chain in aqueous solutions (r_0^2), we found that only the first 5 repeat units of PEO near the grafting point are slightly stretched with $\alpha^2 = 1.01 \sim 1.06$ as shown in Figure S6 in the Supporting Information. This is to be expected as the steric effect is much stronger near the backbone.

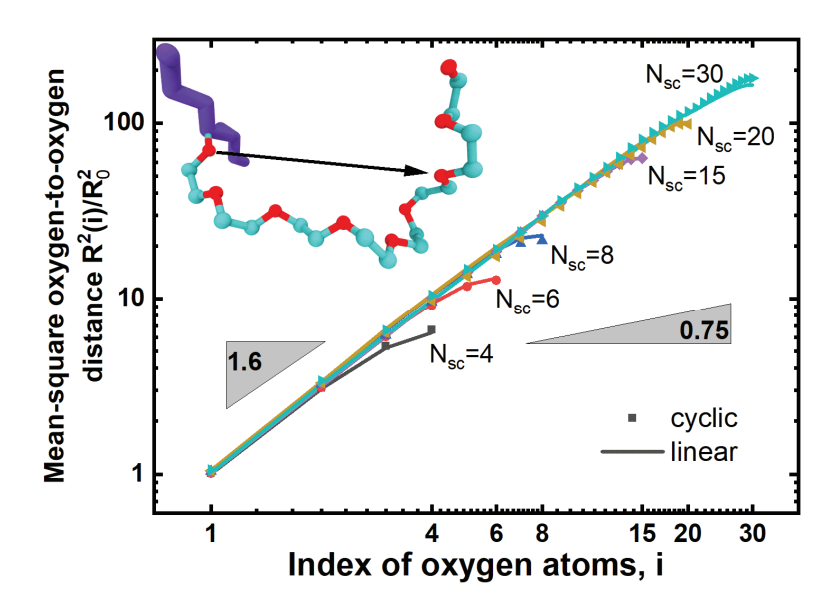


Figure 6: The mean-square distance from the oxygen closest to the backbone to oxygen of the side chain normalized by the average mean-square neighboring oxygen-oxygen distance of PEO in aqueous solutions as a function of the index of the oxygen atoms starting from the grafting point for linear BBPs (lines) and cyclic BBPs (symbols). Inset: snapshot showing a PEO side chain (carbon atoms are shown in cyan, oxygen atoms in red, and the PVA backbone atoms in violet) and the calculated distance, shown in the plot.

BBP shape changes. To quantify the change of shape for linear and cyclic BBPs upon an increase of side chain length, we calculated the chain anisotropy:⁴⁹

$$\kappa^2 = \frac{3}{2} \frac{R_{g1}^4 + R_{g2}^4 + R_{g3}^4}{\left(R_{g1}^2 + R_{g2}^2 + R_{g3}^2\right)^2} - \frac{1}{2}$$
 (3)

where R_{gi}^2 , (i=1, 2, and 3), are the principal moments of the gyration tensor sorted in the order $R_{g1}^2 \ge R_{g2}^2 \ge R_{g3}^2$. The anisotropy describes the mass distribution of a polymer and varies within 0 to1 where $\kappa^2 = 0$ corresponds to a sphere-like shape while $\kappa^2 = 1$ to a rod-like shape.

As shown in Figure 7, the overall anisotropy of cyclic BBPs is much smaller than that of their linear analogs, implying a more compact and more isotropic distribution of mass for cyclic

BBPs. With an increase of the side-chain length, the anisotropy of cyclic BBPs decreases monotonically, approaching zero, indicating a spherical shape, consistent with the snapshots shown in Figure 1 and Figure 7, and the density plot shown in Figure S7 of the Supporting information. As can be seen from these figures, the cyclic BBPs start from a donut-like shape for short grafts, transition to disk-like and then finally become sphere-like or star-like for long grafts. In contrast, for linear BBPs, the anisotropy firstly increases and then decreases upon an increase of the side chain length. To rationalize the dependence of linear BBPs we calculated the principle components of the backbone Rg and aspect ratio Rend,bb/Rg,bb (Figures S1 and S2 of the Supporting Information). For the shortest side chain length N_{sc}=4, the aspect ratio is about 2.48, implying a coil-like conformation (with $\sqrt{6}$ expected for a random coil), consistent with results shown in Figure 4b for short grafts. With an increase of the side chain length, the largest component of Rg and the aspect ratio for the backbone increase (Figures S1 and S2 of the Supporting Information) leading to an increase of anisotropy for the linear BBP as the chain assumes a more expanded conformation. The aspect ratio for the backbone saturates reaching rod-like limit $\sqrt{12}$ at about N_{sc}=8 (Figure S2), at which point the overall BBP anisotropy reaches a maximum (Figure 7). As the side chain length increases further the thickness of the bottle brush continues to increase, thereby decreasing the anisotropy. In the limit of very long side chains exceeding the backbone (N_{sc}>>N_{bb}), the overall shape for linear BBPs would become star-like or spherelike (similar to cyclic BBPs) with a very low anisotropy value. The non-monotonic anisotropy change of the linear BBPs with the increase of side chain length is consistent with a recent Monte Carlo simulation study⁵⁰ of poly(2-(2-bromoisobutyryloxy)ethyl methacrylate)-graft-poly(methyl methacrylate) bottlebrush polymer with N_{bb} =102 and N_{sc} in 28~113.

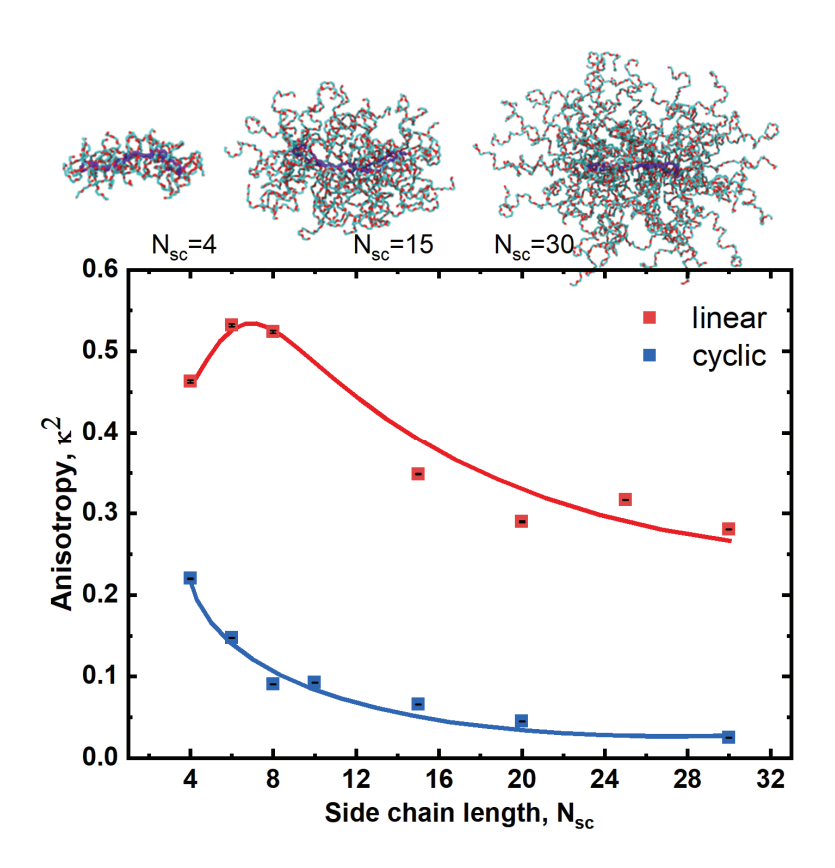


Figure 7: The anisotropy of cyclic and linear BBPs as a function of the PEO side chain length, calculated using Eq. (3). Lines are guides for the eye. Shown on the top are the MD simulation snapshots for cyclic BBPs with side chain lengths $N_{sc} = 4$, 15, and 30. Backbone ($N_{bb}=50$) is colored in violet and side chains are shown in cyan (carbon atoms) and red (oxygen atoms).

To summarize, the linear BBPs undergo a coil to rod/cylinder change of shape upon increasing the graft length and are expected to transition to a sphere-like shape for very long grafts ($N_{sc} >> N_{bb}$); while the cyclic BBPs start from a donut-like then turn into a disk-like shape and finally assume a sphere-like shape for long grafts, as shown in Figure 1, Figure 7, and the density plot in Figure S7 of the Supporting Information.

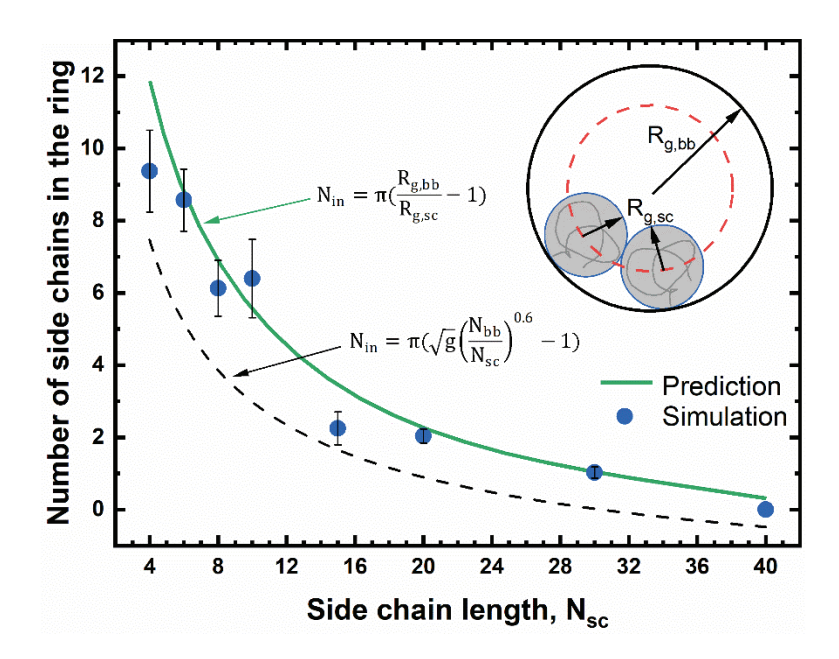


Figure 8: The number of side chains residing inside the cyclic backbone ring as a function of the side chain length obtained in MD simulations (symbols) and the prediction of our model using Eq. (4) (green solid curve). A simplified scaling model, *i.e.*, Eq. (5) is shown as a black dashed line. Inset: schematics of the grafted chains and the backbone ring for the scaling analysis leading to Eq. (4).

Side-chain arrangements in the cyclic BBPs. While for the linear BBPs the side-chain arrangements are symmetric, as is seen from snapshots in Figure 1, for cyclic BBPs, the available space for PEO side-chains inside and outside of the backbone ring is different, potentially leading to different chain arrangement. Moreover, since BBPs have potential applications in drug delivery,^{6,12} it is of fundamental interest and practical importance to quantify the local crowdedness, *e.g.*, the number of chains residing within the backbone ring of the cyclic BBPs, as this clearly could impact encapsulation and/or adsorption of potential payloads. To quantify this property from our simulations, we employed the following criteria to define when a side chain resides inside the ring: (1) the distance between the center of mass (COM) of the backbone ring and the grafting point is larger than the distance between

the COM of the side chain and the COM of the backbone; and (2) the angle (between the COM of the graft to the grafting point and grafting point to the COM of the backbone ring) is less than 60 degrees. The angle criterion was required to ensure that the side chain is located within the interior of the ring, not above or below it, with the angle value chosen was based on the visualization of cyclic BBP accounting for fluctuations in the ring plane and shape. The results obtained from our MD simulations are shown in Figure 8. As is seen the number of chains residing within the ring center significantly decreases with an increase of side chain length. It would be of great value also to develop a predictive model which can provide an evaluation of the number of chains residing within the interior of the cyclic BBP. To this end we estimate the maximum number of side-chains that can fill the inner area of the ring by comparing the circumference of a ring to a cross-sectional diameter of side-chain coil. The schematic for the model is shown in the inset of Figure 8 where the backbone ring with a radius of R_{g,bb} is represented by the black circle and two filled grey circles of a radius R_{g,sc} show two neighboring side chains located inside the ring. The dashed red circle (with a circumference $2\pi(R_{g,bb}-R_{g,sc})$) in comparison to side-chain coil diameter, $2R_{g,sc}$ therefore determines how many side chains can reside inside cyclic BBP:

$$N_{in} = \frac{2\pi (R_{g,bb} - R_{g,sc})}{2R_{g,sc}} = \pi \left(\frac{R_{g,bb}}{R_{g,sc}} - 1\right)$$
(4)

where it's assumed that $R_{g,bb} > R_{g,sc}$.

The values of $R_{g,bb}$ (Figure S8 of the Supporting Information) and $R_{g,sc}$ ($R_{g,sc}$ = 0.13 $N_{sc}^{0.66}$, based on fitting our MD simulation data, Figure S4 of the Supporting Information) are easily obtained from MD simulations and can be used in Eq. (4). The comparison of the prediction

by the scaling model, Eq. (4) and direct MD simulation data is shown in Figure 8, which demonstrates a good agreement between the two. In this model, we assumed that the size of the side chains located inside and outside of the backbone ring is comparable, which is indeed the case, as is seen in our simulations (Figure S9 of the Supporting Information), with the possible exception of the longest side-chains considered, when the number of side chains located inside is too small to achieve statistical accuracy. Based on the results shown in Figure 8, side chains can reside inside the backbone ring only when the grafts are shorter compared to the ring radius ($R_{\rm g,sc} < R_{\rm g,bb}$) and the backbone is far from in the perfect ring conformation. This fact can be used for deriving a simplified scaling model, detailed below.

While our model, Eq. (4) provides a good prediction for the number of side chains residing inside the circumference of the cyclic BPP, for practical purposes the values of $R_{g,bb}$ and $R_{g,sc}$ are not always readily available or known. To deliver a rough estimate as a starting guide for experiments, we note that one can use a good solvent chain model, *i.e.*, the backbone ring $R_{g,bb}$ can be estimated as $R_{g,bb}^2 = gN_{bb}^{1.2}b^2/6$, where the g-factor: $g = R_{g,cyclic}^2/R_{g,linear}^2$ is normally in the range of $0.52 \sim 0.6$ in a good solvent based on experiments, theory and simulations. $R_{g,sc}^2 = R_{g,sc}^2$ for the side chain can be estimated as $R_{g,sc}^2 = N_{sc}^{1.2}b^2/6$. Thus, Eq. (4) can be written as:

$$N_{\rm in} = \pi \left(\sqrt{g} \left(\frac{N_{\rm bb}}{N_{\rm sc}}\right)^{0.6} - 1\right) \tag{5}$$

where it's assumed that both backbone and the side chain have a comparable Kuhn length b. This simplified model gives the prediction shown as the black dashed line in Figure 8 (with g=0.55 used for plotting). While this model slightly underestimates the number of side-

chains located within the ring, it provides a satisfactory agreement proving that it can be used to guide experimental design.

Hydration properties of BBPs. Hydration is very important for water soluble polymers, such as PVA or PEO, because their solubility relies on their ability to form hydrogen bonds with water. To examine and compare the hydration properties of the cyclic and linear BBPs we calculated a) the hydration number per PEO repeat unit, b) the average number of hydrogen bonds with water per PEO repeat unit and c) the water residence correlation function.

The hydration number is defined as the number of water molecules with either its oxygen or hydrogen atoms residing within 0.35 nm from the BBP atoms. The hydration number per PEO repeat unit averaged over time (10 ns) and all chains is shown in Figure 9a as a function of the side chain length. As is seen, the hydration number increases with the side chain length for both cyclic and linear BBPs, due to the increase of accessible volume for water away from the backbone especially for BBPs with longer side chains. It also shows that only for the longest grafts on linear BBPs the hydration number reaches about 5.8 as expected for PEO in aqueous solutions.³⁷ Compared to their linear analogs, cyclic BBPs have a somewhat smaller hydration number due to larger chain crowding especially in the region close to the backbone ring, as discussed above.

The average number of hydrogen bonds formed between the BBPs and water is found to be less sensitive to the backbone topology (Figure S6b of the Supporting Information), as it depends on the local water concentration near PEO oxygens, similar to what was found for

a planar PEO brush.⁵⁴ Near the backbone the polymer concentration is higher and accordingly water concentration is lower leading to somewhat lower degree of hydrogen bonding with water with negligible difference between linear and cyclic BBPs (Figure S6b of the Supporting Information) The PEO segments close to the linear or cyclic BBP backbone within about 5 repeat units are somewhat less hydrated while the remaining segments are well hydrated with an average 1.2 hydrogen bonds with water as expected for PEO in an aqueous solution.³⁷ We note that the intramolecular hydrogen bonding via hydroxyl groups at the end of the PEO side chains is very low, about $2.5\sim2.6$ hydrogen bonds per BBP or 0.0017 per PEO monomer for N_{sc} =30) compared to the PEO-water hydrogen bonding and also independent of BBP topology (linear or cyclic).

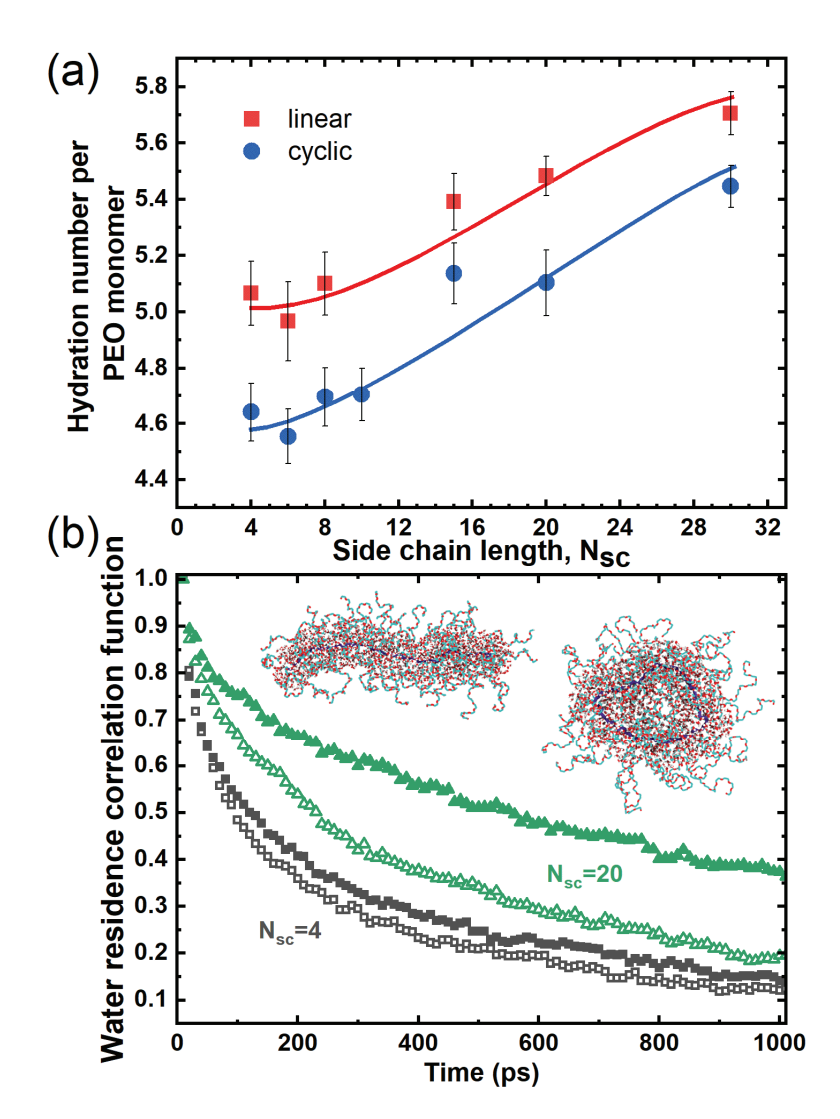


Figure 9: (a) The average hydration number per PEO monomer as a function of the side chain length for linear and cyclic BBPs. Lines are guides for the eye. (b) The water residence correlation function for the linear (open symbols) and cyclic (solid symbols) BBPs with side chain length N_{sc} = 4 (black), and 20 (green) calculated using Eq. (6). Inset: screenshots for the hydration layer (water is shown in red and white) within 1nm distance to the backbone of the linear and cyclic BBPs.

While the hydration number and number of hydrogen bonds are informative for static hydration properties, they do not provide any dynamic information about water exchange.

To characterize the stability of water residing within a 1 nm shell from the backbones of

BBPs (see the snapshots in Figure 9b), we calculated the water residence correlation function:

$$C(t) = \langle \frac{N_{w}(t)}{N_{w}(0)} \rangle \tag{6}$$

where $N_w(0)$ is the number of waters residing within the 1nm shell of the backbone at t=0 and $N_w(t)$ is the number of these same "marked" waters remaining in the shell after time t. The comparison of the water residence correlation functions for the cyclic BBPs and their linear counterparts as functions of time are shown in Figure 9b. As is seen, water in the shell of cyclic BBP decays slower, indicating that the water layer near the cyclic BBP is more dynamically stable than that near the linear BBP with the same graft length. This is due to the compactness of the cyclic BBP backbone leading to enhanced crowding of the PEO sidechains. This difference is more significant for longer side chains. As can be seen, for the short grafts N_{sc} =4, both cyclic and linear BBPs have similar decay, with about 15% and 12% initial waters left after 1ns. While for the longer grafts, N_{sc} =20, there are about 35% waters remain for cyclic BBPs and 20% for the linear BBPs.

Therefore, both backbone topology and graft length affect the hydration number and water mobility near the BBPs, leading to less hydrated cyclic BBPs with more stable hydration layer around the backbone compared to the linear BBPs.

CONCLUSIONS

Using atomistic MD simulations, we have investigated the structural and hydration properties of cyclic and linear BBPs to reveal the dependence of these properties on the backbone topology and the graft length. We found that cyclic BBPs are more compact and

explore a narrower conformational space compared to their linear analogs (Figure 1 and Figure 2) until the limit of very long side-chains is reached (N_{sc}>>N_{bb}) when both linear and cyclic BBPs become star-like. The radius of gyration of cyclic BBPs increases with an increase of the side chain length at somewhat slower rate than the linear BBPs (Figure 3), due to the difference in backbone topology, while in the limit of long side-chains both cyclic and linear BBPs follow the same scaling behavior $R_g \sim N_{sc}^{0.58}$, as previously observed experimentally for linear BBPs. 41,42 For short grafts the backbone rigidity increases upon an increase of the graft length (Figure 4) with a similar scaling of the persistence length (in the limit of a long backbone $N_{bb} >> N_{sc})$ for both cyclic and linear BBPs: $l_p \sim N_{sc}^{0.54}.$ In the long side chain limit the persistence length of cyclic BBP saturates, but the persistence length of the linear BBPs strongly increases approaching the scaling $l_p{\sim}N_{sc}^{15/8}\text{, as predicted by Fredrickson}^{26}$ and observed in CGMD simulations¹⁷ (Figure 5). In both linear and cyclic BBPs the side chains are only slightly stretched with the expansion ratio (R_{g,sc}/R_{g0}) of about 1.1 compared to that in aqueous solutions (for N_{sc}=20) and demonstrate little dependence on the backbone topology (Figure 6). Side chain segments near the backbone are more stretched due to steric effects while assuming similar conformation to PEO chains in aqueous solutions (expansion ratio about 1.0) further away from the backbone (Figure S6a of the Supporting Information). The topology of the backbone and side chain length affect the overall shape of the cyclic and linear BBPs (Figure 7). Upon a graft length increase cyclic BBPs change shape from donutlike to sphere-like or star-like, while the linear BBPs shape transforms from a coil-like (N_{sc} << N_{bb}) to rod-like or cylinder-like and is expected to transform into star-like for very long grafts ($N_{sc} >> N_{bb}$).

To quantify the side-chain spatial distribution in cyclic BBPs, we have proposed a scaling model to evaluate the fraction of side-chains located inside (near the center of) the cyclic BBPs (Figure 8 and Eq.(4)). The model shows that the side-chain fraction residing inside the backbone ring depends on the size of the ring and decreases with an increase of graft length. A more general, but less precise model is also presented (Eq. (5)) for the case that the specific polymer parameters are not known for the cyclic BBP components. These predictions can be used for guidance in designing payload bearing carriers based on cyclic BBPs, *e.g.*, for drug or nanoparticle delivery or solubilization.

The aforementioned structural differences between cyclic and linear BBPs result in different hydration properties (Figure 9). As cyclic BBPs are more compact the hydration number per monomer of PEO side-chain is smaller than that for the linear BBPs and in both cases increases as the side-chain length increases, as the accessible volume for water expands. The hydrogen bonding between BBPs and water is somewhat reduced near the backbone (about 0.8~0.9) while away from it reaches 1.2 hydrogen bonds per PEO repeat unit as expected for well-hydrated PEO in aqueous solution (Figure S6b of the Supporting Information). Furthermore, the compactness of cyclic BBP results in more stable hydration shell within 1nm of cyclic BBP backbone compared to that for the linear BBPs. These observations can have important implications for cyclic bottle brush solubility, their potential for biomedical applications (*e.g.*, drug or nanoparticle encapsulation) and stability against self-aggregation or interactions with co-solutes.

ASSOCIATED CONTENT

The Supporting Information is available free of charge at ...

Computer simulation details of the simulation box sizes; the principle components of the

radius of gyration for cyclic and linear backbones; the end-to-end distance and aspect ratio

of the backbone of linear BBPs; the schematics for persistence length estimate at long graft

limit; the radius of gyration, end-to-end distance and aspect ratio of the side chains of linear

and cyclic BBPs, all as functions of the PEO side chain length; the expansion ratio and the

average number of hydrogen bonds per PEO monomer for linear and cyclic BBPs as functions

of the oxygen atom index starting from the backbone; the density plots for the linear and

cyclic BBPs with different side chain lengths; the radius of gyration of the backbone ring and

the radius of gyration of the side chains (outside and inside the ring) for cyclic BBPs as a

function of side chain length.

AUTHOR INFORMATION

Corresponding Author:

Elena E. Dormidontova - Polymer Program, Institute of Materials Science and Physics

Department, University of Connecticut, Storrs, Connecticut 06269, United States. Orcid:

0000-0002-7669-8957. Email: elena@uconn.edu

ACKNOWLEDGMENTS

This research is supported by the National Science Foundation under Grant No. CHE-

2004072. Fruitful discussions with Professor Douglas Adamson of this research area are

29

gratefully acknowledged. This work used the Extreme Science and Engineering Discovery Environment (XSEDE) through allocation TG-MAT210004 (supported by National Science Foundation grant number ACI-1548562) and the Expanse HPC at San Diego Supercomputer Center through allocation MAT-210004 from the Advanced Cyberinfrastructure Coordination Ecosystem: Services & Support (ACCESS) program, which is supported by National Science Foundation grants #2138259, #2138286, #2138307, #2137603, and #2138296.

REFERENCES

- (1) Sheiko, S. S.; Sumerlin, B. S.; Matyjaszewski, K. Cylindrical Molecular Brushes: Synthesis, Characterization, and Properties. *Prog. Polym. Sci.* **2008**, *33* (7), 759–785, DOI 10.1016/j.progpolymsci.2008.05.001.
- (2) Verduzco, R.; Li, X.; Pesek, S. L.; Stein, G. E. Structure, Function, Self-Assembly, and Applications of Bottlebrush Copolymers. *Chem. Soc. Rev.* **2015**, *44* (8), 2405–2420, DOI 10.1039/c4cs00329b.
- (3) Zhao, B. Shape-Changing Bottlebrush Polymers. *J. Phys. Chem. B* **2021**, *125* (24), 6373–6389, DOI 10.1021/acs.jpcb.1c01819.
- (4) Daniel, W. F. M.; Burdyńska, J.; Vatankhah-Varnoosfaderani, M.; Matyjaszewski, K.; Paturej, J.; Rubinstein, M.; Dobrynin, A. V.; Sheiko, S. S. Solvent-Free, Supersoft and Superelastic Bottlebrush Melts and Networks. *Nat. Mater.* **2016**, *15* (2), 183–189, DOI 10.1038/nmat4508.
- (5) Detappe, A.; Nguyen, H. V.-T.; Jiang, Y.; Agius, M. P.; Wang, W.; Mathieu, C.; Su, N. K.; Kristufek, S. L.; Lundberg, D. J.; Bhagchandani, S.; Ghobrial, I. M.; Ghoroghchian, P. P.; Johnson, J. A. Molecular Bottlebrush Prodrugs as Mono- and Triplex Combination Therapies for Multiple Myeloma. *Nat. Nanotechnol.* **2023**, DOI 10.1038/s41565-022-01310-1.
- (6) Tu, X. Y.; Meng, C.; Wang, Y. F.; Ma, L. W.; Wang, B. Y.; He, J. L.; Ni, P. H.; Ji, X. L.; Liu, M. Z.; Wei, H. Fabrication of Thermosensitive Cyclic Brush Copolymer with Enhanced Therapeutic Efficacy for Anticancer Drug Delivery. *Macromol. Rapid Commun.* **2018**, 39 (5), 1–8, DOI 10.1002/marc.201700744.
- (7) Xu, P.; Wang, S.; Lin, A.; Min, H.-K.; Zhou, Z.; Dou, W.; Sun, Y.; Huang, X.; Tran, H.; Liu, X. Conductive and Elastic Bottlebrush Elastomers for Ultrasoft Electronics. *Nat. Commun.* **2023**, *14* (1), 623, DOI 10.1038/s41467-023-36214-8.

- (8) Xie, R.; Lapkriengkri, I.; Pramanik, N. B.; Mukherjee, S.; Blankenship, J. R.; Albanese, K.; Wang, H.; Chabinyc, M. L.; Bates, C. M. Hydrogen-Bonding Bottlebrush Networks: Self-Healing Materials from Super-Soft to Stiff. *Macromolecules* **2022**, *55* (23), 10513–10521, DOI 10.1021/acs.macromol.2c01886.
- (9) Zhou, J.; Yang, J.; Ishaq, M. W.; Li, L. Study of Linear and Cyclic Graft Polystyrenes with Identical Backbone Contour in Dilute Solutions: Preparation, Characterization, and Conformational Properties. *Macromolecules* **2022**, *55* (4), 1398–1411, DOI 10.1021/acs.macromol.1c02029.
- (10) Xu, L.; Gao, B.; Xu, X.; Zhou, L.; Liu, N.; Wu, Z. Controlled Synthesis of Cyclic-Helical Polymers with Circularly Polarized Luminescence. *Angew. Chemie* **2022**, *134* (28), DOI 10.1002/ange.202204966.
- (11) Schappacher, M.; Deffieux, A. Synthesis of Macrocyclic Copolymer Brushes and Their Self-Assembly into Supramolecular Tubes. *Science* (80-.). **2008**, 319 (5869), 1512–1515, DOI 10.1126/science.1153848.
- (12) Liu, Z.; Huang, Y.; Zhang, X.; Tu, X.; Wang, M.; Ma, L.; Wang, B.; He, J.; Ni, P.; Wei, H. Fabrication of Cyclic Brush Copolymers with Heterogeneous Amphiphilic Polymer Brushes for Controlled Drug Release. *Macromolecules* **2018**, *51* (19), 7672–7679, DOI 10.1021/acs.macromol.8b00950.
- (13) Schappacher, M.; Deffieux, A. Atomic Force Microscopy Imaging and Dilute Solution Properties of Cyclic and Linear Polystyrene Combs. *J. Am. Chem. Soc.* **2008**, *130* (44), 14684–14689, DOI 10.1021/ja804780s.
- (14) Yang, J.; Wang, R.; Xie, D. Aqueous Self-Assembly of Amphiphilic Cyclic Brush Block Copolymers as Asymmetry-Tunable Building Blocks. *Macromolecules* **2019**, *52* (18), 7042–7051, DOI 10.1021/acs.macromol.9b01393.
- (15) Zhang, Z.; Carrillo, J. M. Y.; Ahn, S. K.; Wu, B.; Hong, K.; Smith, G. S.; Do, C. Atomistic Structure of Bottlebrush Polymers: Simulations and Neutron Scattering Studies. *Macromolecules* **2014**, *47* (16), 5808–5814, DOI 10.1021/ma500613c.
- (16) Sunday, D. F.; Chremos, A.; Martin, T. B.; Chang, A. B.; Burns, A. B.; Grubbs, R. H. Concentration Dependence of the Size and Symmetry of a Bottlebrush Polymer in a Good Solvent. *Macromolecules* **2020**, *53* (16), 7132–7140, DOI 10.1021/acs.macromol.0c01181.
- (17) Chatterjee, D.; Vilgis, T. A. Scaling Laws of Bottle-Brush Polymers in Dilute Solutions. *Macromol. Theory Simulations* **2016**, *25* (6), 518–523, DOI 10.1002/mats.201600074.
- (18) Feuz, L.; Leermakers, F. A. M.; Textor, M.; Borisov, O. Bending Rigidity and Induced Persistence Length of Molecular Bottle Brushes: A Self-Consistent-Field Theory. *Macromolecules* **2005**, *38* (21), 8891–8901, DOI 10.1021/ma050871z.
- (19) Hsu, H. P.; Paul, W. A Fast Monte Carlo Algorithm for Studying Bottle-Brush Polymers. *Comput. Phys. Commun.* **2011**, *182* (10), 2115–2121, DOI 10.1016/j.cpc.2011.05.005.

- (20) Saariaho, M.; Subbotin, A.; Szleifer, I.; Ikkala, O.; Ten Brinke, G. Effect of Side Chain Rigidity on the Elasticity of Comb Copolymer Cylindrical Brushes: A Monte Carlo Simulation Study. *Macromolecules* **1999**, *32* (13), 4439–4443, DOI 10.1021/ma990307m.
- (21) Yethiraj, A. A Monte Carlo Simulation Study of Branched Polymers. *J. Chem. Phys.* **2006**, *125* (20), DOI 10.1063/1.2374884.
- (22) Theodorakis, P. E.; Hsu, H. P.; Paul, W.; Binder, K. Computer Simulation of Bottle-Brush Polymers with Flexible Backbone: Good Solvent versus Theta Solvent Conditions. *J. Chem. Phys.* **2011**, *135* (16), DOI 10.1063/1.3656072.
- (23) Dutta, S.; Wade, M. A.; Walsh, D. J.; Guironnet, D.; Rogers, S. A.; Sing, C. E. Dilute Solution Structure of Bottlebrush Polymers. *Soft Matter* **2019**, *15* (14), 2928–2941, DOI 10.1039/c9sm00033j.
- (24) Mohammadi, E.; Joshi, S. Y.; Deshmukh, S. A. A Review of Computational Studies of Bottlebrush Polymers. *Comput. Mater. Sci.* **2021**, *199* (February), 110720, DOI 10.1016/j.commatsci.2021.110720.
- (25) Cao, Z.; Carrillo, J. M. Y.; Sheiko, S. S.; Dobrynin, A. V. Computer Simulations of Bottle Brushes: From Melts to Soft Networks. *Macromolecules* **2015**, *48* (14), 5006–5015, DOI 10.1021/acs.macromol.5b00682.
- (26) Fredrickson, G. H. Surfactant-Induced Lyotropic Behavior of Flexible Polymer Solutions. *Macromolecules* **1993**, *26* (11), 2825–2831, DOI 10.1021/ma00063a029.
- (27) Birshtein, T. M.; Borisov, O. V.; Zhulina, Y. B.; Khokhlov, A. R.; Yurasova, T. A. Conformations of Comb-like Macromolecules. *Polym. Sci. U.S.S.R.* **1987**, *29* (6), 1293–1300, DOI 10.1016/0032-3950(87)90374-1.
- (28) Saariaho, M.; Ikkala, O.; Szleifer, I.; Erukhimovich, I.; ten Brinke, G. On Lyotropic Behavior of Molecular Bottle-Brushes: A Monte Carlo Computer Simulation Study. *J. Chem. Phys.* **1997**, *107* (8), 3267–3276, DOI 10.1063/1.474677.
- (29) Saariaho, M.; Szleifer, I.; Ikkala, O.; ten Brinke, G. Extended Conformations of Isolated Molecular Bottle-Brushes: Influence of Side-Chain Topology. *Macromol. Theory Simulations* **1998**, 7 (2), 211–216, DOI 10.1002/(SICI)1521-3919(19980301)7:2<211::AID-MATS211>3.0.CO;2-A.
- (30) Subbotin, A.; Saariaho, M.; Ikkala, O.; Ten Brinke, G. Elasticity of Comb Copolymer Cylindrical Brushes. *Macromolecules* **2000**, *33* (9), 3447–3452, DOI 10.1021/ma991031l.
- (31) Subbotin, A. V.; Semenov, A. N. Spatial Self-Organization of Comb Macromolecules. *Polym. Sci. Ser. A* **2007**, *49* (12), 1328–1357, DOI 10.1134/S0965545X07120085.
- (32) Nakamura, Y.; Norisuye, T. Backbone Stiffness of Comb-Branched Polymers. *Polym. J.* **2001**, *33* (11), 874–878, DOI 10.1295/polymj.33.874.

- (33) Humphrey, W.; Dalke, A.; Schulten, K. VMD: Visual Molecular Dynamics. *J. Mol. Graph.* **1996**, *14* (1), 33–38, 27–28, DOI 10.1016/0263-7855(96)00018-5.
- (34) Van Der Spoel, D.; Lindahl, E.; Hess, B.; Groenhof, G.; Mark, A. E.; Berendsen, H. J. C. GROMACS: Fast, Flexible, and Free. *J. Comput. Chem.* **2005**, *26* (16), 1701–1718, DOI 10.1002/jcc.20291.
- (35) Towns, J.; Cockerill, T.; Dahan, M.; Foster, I.; Gaither, K.; Grimshaw, A.; Hazlewood, V.; Lathrop, S.; Lifka, D.; Peterson, G. D.; Roskies, R.; Scott, J. ray; Wilkins-Diehr, N. Accelerating Scientific Discovery. *Comput. Sci. Eng.* **2014**, *16* (5), 62–74.
- (36) Jorgensen, W. L.; Maxwell, D. S.; Tirado-Rives, J. Development and Testing of the OPLS All-Atom Force Field on Conformational Energetics and Properties of Organic Liquids. *J. Am. Chem. Soc.* **1996**, *118* (45), 11225–11236, DOI 10.1021/ja9621760.
- (37) Dahal, U. R.; Dormidontova, E. E. The Dynamics of Solvation Dictates the Conformation of Polyethylene Oxide in Aqueous, Isobutyric Acid and Binary Solutions. *Phys. Chem. Chem. Phys.* **2017**, *19* (15), 9823–9832, DOI 10.1039/c7cp00526a.
- (38) Berendsen, H. J. C.; Grigera, J. R.; Straatsma, T. P. The Missing Term in Effective Pair Potentials. *J. Phys. Chem.* **1987**, *91* (24), 6269–6271, DOI 10.1021/j100308a038.
- (39) Rouault, T.; Borisov, O. V. Comb-Branched Polymers: Monte Carlo Simulation and Scaling. *Macromolecules* **1996**, *29* (7), 2605–2611, DOI 10.1021/ma951126x.
- (40) Pan, X.; Ding, M.; Li, L. Experimental Validation on Average Conformation of a Comblike Polystyrene Library in Dilute Solutions: Universal Scaling Laws and Abnormal SEC Elution Behavior. *Macromolecules* **2021**, *54* (23), 11019–11031, DOI 10.1021/acs.macromol.1c01029.
- (41) Zhang, M.; Breiner, T.; Mori, H.; Müller, A. H. E. Amphiphilic Cylindrical Brushes with Poly(Acrylic Acid) Core and Poly(n-Butyl Acrylate) Shell and Narrow Length Distribution. *Polymer (Guildf).* **2003**, *44* (5), 1449–1458, DOI 10.1016/S0032-3861(02)00774-7.
- (42) Zhang, B.; Gröhn, F.; Pedersen, J. S.; Fischer, K.; Schmidt, M. Conformation of Cylindrical Brushes in Solution: Effect of Side Chain Length. *Macromolecules* **2006**, *39* (24), 8440–8450, DOI 10.1021/ma0613178.
- (43) Grest, G. S.; Kremer, K.; Witten, T. A. Structure of Many-Arm Star Polymers: A Molecular Dynamics Simulation. *Macromolecules* **1987**, *20* (6), 1376–1383, DOI 10.1021/ma00172a035.
- (44) Hsu, H. P.; Nadler, W.; Grassberger, P. Scaling of Star Polymers with 1-80 Arms. *Macromolecules* **2004**, *37* (12), 4658–4663, DOI 10.1021/ma0355958.
- (45) Dahal, U.; Dormidontova, E. E. Chain Conformation and Hydration of Polyethylene Oxide Grafted to Gold Nanoparticles: Curvature and Chain Length Effect. *Macromolecules* **2020**, *53* (19), 8160–8170, DOI 10.1021/acs.macromol.0c01499.

- (46) Devanand, K.; Selser, J. C. Asymptotic Behavior and Long-Range Interactions in Aqueous Solutions of Poly(Ethylene Oxide). *Macromolecules* **1991**, *24* (22), 5943–5947, DOI 10.1021/ma00022a008.
- (47) Dill, K. A.; Bromberg, S.; Stigter, D. Polymer Solutions. In *Molecular Driving Forces*; Garland Science, 2010; Vol. 3, pp 643–657, DOI 10.4324/9780203809075-32.
- (48) Hsu, H. P.; Paul, W.; Binder, K. One- And Two-Component Bottle-Brush Polymers: Simulations Compared to Theoretical Predictions. *Macromol. Theory Simulations* **2007**, *16* (7), 660–689, DOI 10.1002/mats.200700031.
- (49) Theodorou, D. N.; Suter, U. W. Shape of Unperturbed Linear Polymers: Polypropylene. *Macromolecules* **1985**, *18* (6), 1206–1214, DOI 10.1021/ma00148a028.
- (50) Raj, W.; Hałagan, K.; Kadłubowski, S.; Maczugowska, P.; Szutkowski, K.; Jung, J.; Pietrasik, J.; Jurga, S.; Sikorski, A. The Structure and Dynamics of Bottlebrushes: Simulation and Experimental Studies Combined. *Polymer (Guildf).* **2022**, *261* (July), 125409, DOI 10.1016/j.polymer.2022.125409.
- (51) Takano, A.; Ohta, Y.; Masuoka, K.; Matsubara, K.; Nakano, T.; Hieno, A.; Itakura, M.; Takahashi, K.; Kinugasa, S.; Kawaguchi, D.; Takahashi, Y.; Matsushita, Y. Radii of Gyration of Ring-Shaped Polystyrenes with High Purity in Dilute Solutions. *Macromolecules* **2012**, *45* (1), 369–373, DOI 10.1021/ma202031w.
- (52) Douglas, J.; Freed, K. F. Renormalization and the Two-Parameter Theory. 1. *Macromolecules* **1984**, *17* (11), 2344–2354, DOI 10.1021/ma00141a026.
- (53) Chen, Y. Der. On the Ring-to-Chain Ratios of Radii of Gyration and Sedimentation Coefficients of Polymers of the Freely Jointed Model: Monte Carlo Calculations and the ε Method. *J. Chem. Phys.* **1983**, *78* (8), 5191–5196, DOI 10.1063/1.445389.
- (54) Dahal, U. R.; Wang, Z.; Dormidontova, E. E. Hydration and Mobility of Poly(Ethylene Oxide) Brushes. *Macromolecules* **2017**, *50* (17), 6722–6732, DOI 10.1021/acs.macromol.7b01369.